AIAA JOURNAL
Vol. 49, No. 2, February 2011

Technical Notes

Density Field Measurements of a Supersonic Impinging Jet with Microjet Control

L. Venkatakrishnan*
National Aerospace Laboratories, Bangalore 560 017, India
and
Alex Wiley,† Rajan Kumar,‡ and Farrukh Alvi§
Florida A&M University and Florida State University, Tallahassee, Florida 32310

DOI: 10.2514/1.J050511

Nomenclature

D	=	nozzle diameter at the throat, 2.54 cm
h	=	distance between the nozzle exit and ground plane
NPR	=	nozzle pressure ratio, P_o/P_a
P	=	jet pressure
TR	=	temperature ratio, T_o/T_a
T	=	jet temperature
ρ	=	jet density

Subscripts

a	=	ambient conditions
o	=	stagnation conditions

I. Introduction

FLOW impingement of a supersonic jet on a solid surface produces a highly turbulent and complex flowfield with a multiple shock systems and viscous-inviscid interactions [1,2]. Many examples of such a flowfield can be found in engineering applications such as: the launch of a rocket, takeoff and landing of a short takeoff and vertical landing (STOVL) aircraft and the exhaust of an aircraft on a carrier deck impinging on a deflector plate. Very often this unsteady flowfield has a detrimental effect on the performance of the aerodynamic system where such flows occur; making its control highly desirable. A better understanding of the complex flowfield associated with impinging jets is therefore needed to design efficient control systems which can mitigate its effects on the aircraft/vehicles. As an example, STOVL aircraft during hover produce highly oscillatory impinging jets on the landing surface [3]. This leads to severe ground erosion of the landing surface, lift loss due to entrainment of high speed flow near the nozzle exit, very high unsteady loads on the nearby structures and hot gas ingestion into the engine inlets. Supersonic impinging jets are a cause of concern due to sonic fatigue failure of the aircraft structure and a major source of noise pollution for the personnel in the aircraft vicinity.

Over the last decade, research at the Advanced Aero-Propulsion Laboratory (AAPL) has successfully demonstrated the application of an array of high momentum microjets, appropriately placed near the nozzle exit, to effectively control supersonic impinging jets [4–10]. This control-on-demand technique has many advantages over traditional passive and active control methods and has been proven to be successful over a range of geometric and flow conditions. With the help of particle image velocimetry (PIV) measurements [9], it has been shown that one of the primary mechanisms behind this control scheme is the introduction of streamwise vorticity at the expense of azimuthal vorticity of the main jet. A reduction in the primary shear layer instability/receptivity (due to shear layer thickening), an attenuation of upstream propagating acoustic waves and the disruption of spatial coherence between large-scale structures and acoustic field lead to an overall attenuation in the feedback loop. However, many questions for both uncontrolled and controlled impinging jets remain.

The answer, in part, lies in a better understanding of the flow physics, especially in the region near the nozzle exit where microjets most directly influence the shear layer properties of the impinging jet. It is felt that a detailed look at the density field with and without microjet control, undocumented to-date, can provide further insight into the flow behavior. Hence, an attempt to measure the density field using the background oriented Schlieren (BOS) technique is carried out in this study. BOS is a technique used to obtain quantitative density fields in a flow employing correlation and topographic algorithms while requiring minimal/simple hardware. The validation of the BOS technique was carried out by Venkatakrishnan and Meier [11], who combined it with filtered back projection tomography to provide the mean density field in a 2-D plane. The extraction of a desired plane using filtered back projection tomography was demonstrated by Venkatakrishnan [12], who mapped the center plane of both a four-jet cruciform configuration and a highly underexpanded supersonic axisymmetric jet, and more recently Venkatakrishnan and Suriyanarayanan [13] applied BOS to supersonic separated flow past an afterbody nozzle. In this paper we demonstrate the application of BOS on a supersonic free and an impinging jet at ideally expanded jet conditions. The effect of microjet control on the density field of both free and impinging jet is also presented in the paper.

II. Experimental Methods

A. Test Facilities and Models

The experiments were carried out in the STOVL supersonic jet facility of the AAPL located at the Florida State University in Tallahassee. This facility is mainly used to study jet-induced phenomena on STOVL aircraft during hover. To simulate different aircraft-to-ground distances, the ground plane is mounted on a hydraulic lift and can be moved vertically. High-pressure compressed air ($\sim$110 bar) stored in large storage tanks (10 m^3) and is used to drive the facility. The measurements were made at both design and off-design conditions of a Mach 1.5 jet issuing from a converging-diverging axisymmetric nozzle.

A circular plate of diameter 25.4 cm ($=10D$) was flush mounted with the nozzle exit. This plate, henceforth referred as lift plate, represents a generic aircraft planform and has a central hole, equal to the nozzle exit diameter, through which the jet is issued. An

Presented as Paper 2010-102 at the 48th AIAA Aerospace Sciences Meeting Including the New Horizons Forum and Aerospace Exposition, Orlando, FL, 4–7 January 2010; received 16 March 2010; revision received 7 September 2010; accepted for publication 22 October 2010.

*Scientist, Experimental Aerodynamics Division, Council of Scientific and Industrial Research. Associate Fellow AIAA.
†Research Assistant, Department of Mechanical Engineering, Florida Center for Advanced Aero-Propulsion. Student Member AIAA.
‡Research Scientist, Department of Mechanical Engineering, Florida Center for Advanced Aero-Propulsion. Senior Member AIAA.
§Professor, Department of Mechanical Engineering, Florida Center for Advanced Aero-Propulsion. Associate Fellow AIAA.

aluminum plate with dimensions 1 m × 1 m × 25 mm represents the ground plane and is mounted on the hydraulic lift directly under the nozzle exit. A sketch and images of the facility along with the test setup used in the present experiments are shown in Fig. 1. More details on the test facility can be found in [10].

B. BOS Technique and Setup

The principle of the technique is the variation of refractive index due to density gradients in the flow (Fig. 2). The determination of the density field using BOS thus involves the following steps:

1) Calculation of displacements of the background pattern which is imaged through the flow of interest. This is done through an in-house PIV-type cross-correlation algorithm. These displacements are proportional to the vectors of the density gradient at each point.

2) Calculation of the line-of-sight integrated density field by solution of the Poisson equation, based on the above displacement.

3) Use of optical tomography (filtered back projection) to determine the density field in the actual plane of interest. The reconstruction of the entire field is achieved by inverse tomography.

In the first step, an image is taken of a random dot pattern with the air (phase object) at rest, i.e., at the "no flow" state. The second image is taken in the presence of the flow containing density gradients. Cross-correlation of the two images yields the displacements of the particles in the x and y directions. Here, x is along the radial direction and y is along the jet axis, also the axis of symmetry for the present case, (with origin at nozzle exit) and perpendicular to the line-of-sight direction z.

Since the deflection of a single beam contains information about the spatial gradient of the refractive index (n) integrated along the axial path, the image deflection ε is defined as

$$\varepsilon = \frac{1}{n_o}\int_{Z_D-\Delta Z_D}^{Z_D+\Delta Z_D} \frac{\delta n}{\delta y}\,\mathrm{d}z \tag{1}$$

with the assumption that the half-width of the region of density gradient $\Delta Z_D \ll Z_D$.

Further, it is seen from geometry (Fig. 2) that the virtual image displacement $\Delta y'$ is related to the image displacement Δy by the lens distance from the background Z_B and the image distance from the lens Z_i, which can be replaced for large Z_B by the focal length f of the lens (Meier [14]):

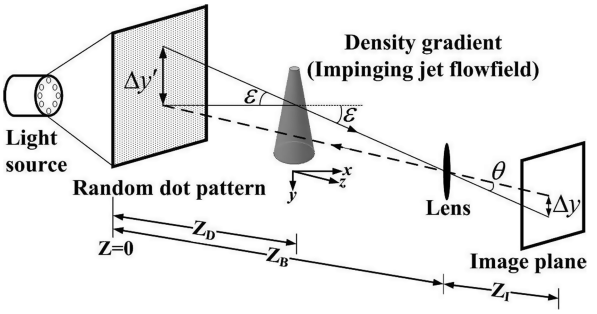

Fig. 2 Optical path for density gradient measurements by light deflection.

$$\frac{\Delta y'}{Z_B} = \frac{\Delta y}{Z_i} = \frac{\Delta y}{f} \tag{2}$$

For small deflection angles, ε can be approximated as

$$\varepsilon = \frac{\Delta y'}{Z_D}$$

and hence

$$\varepsilon = \frac{\Delta y Z_B}{Z_D f} \tag{3}$$

From Eqs. (2) and (3) it follows that for a given flowfield, the shift of the background and the sensitivity ($(\Delta y/\mathrm{gradn}) \sim Z_D Z_B$) increases with increasing distance of the background from the density gradient. Increasing focal length f is compensated by increasing the distance between the camera and the background.

It thus follows that the obtained displacements are the density gradients at each point in the field. The gradients of this displacement field yield an elliptic partial differential equation also known as Poisson equation, solution of which yields the line-of-sight integrated density distribution, which is a projection of the three-dimensional density field in the direction of viewing. The density distribution in a given plane is then reconstructed by means of a (filtered back projection) transformation from this projection. The reader is referred to Venkatakrishnan and Meier [11] for a derivation of the reconstruction function and further details on BOS technique.

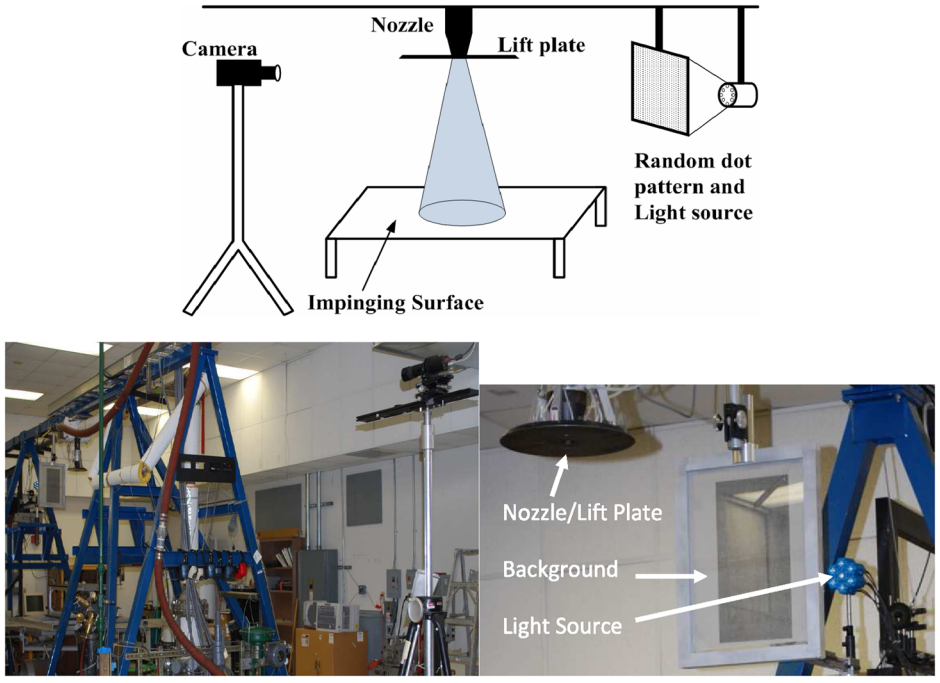

Fig. 1 Experimental setup and a closer view of the BOS apparatus.

Figure 1 also shows a closer view of the BOS apparatus as used in the present facility. The background was a normalized random dot pattern printed out on tracing paper and sandwiched between two glass panels to minimize vibration. The illumination was by means of an light-emitting diode cluster (Model 07LED, IDT Inc). The background was imaged using a SharpVISION 1400DE camera whose exposure time was reduced to 50 μs.

C. Test Conditions

The experiments were conducted at a nozzle pressure ratio (NPR $= P_o/P_a$) of 3.7 corresponding to a nearly ideally expanded jet flow conditions. The air is heated using an inline flow heater to maintain a stagnation temperature of 300 K at the nozzle exit, resulting in a temperature ratio (TR = stagnation temperature/ambient temperature) of 1.0. The test Reynolds number based on the exit velocity and the nozzle diameter of the jet was 7×10^5. Sixteen microjet actuators were flush-mounted circumferentially on the lift plate around the main jet to implement active flow control. The jets issued from 400 μm diameter stainless steel tubes mounted at an inclination of 60° with respect to the main jet axis. The supply for the microjets was provided from a compressed nitrogen cylinder through a plenum chamber. These microjets were operated at a pressure of 100 psia and the combined mass flux from all the microjets was less than 0.5% of the primary jet mass flux. The ground plane was positioned at three different distances from the lift plate, $h = 40D$ representing the freejet and the two cases of impinging jet as $4.5D$ and $4D$.

III. Results and Discussion

As stated earlier, the aim of the present study is to attempt gain a better understanding of some of the flow physics through a detailed examination of the density field of the flow. This is carried out by both qualitative (shadowgraph) and quantitative (BOS) means. Results from flow visualization are first presented followed by quantitative density fields derived from BOS measurements. For all test cases, results in the absence and presence of control will be compared to discern changes brought about in the density field due to the activation of microjets.

A. Flow Visualization Using Conventional Shadowgraph

A conventional shadowgraph technique was used by [10] to first visualize the global flow features associated with impinging jet flow and its response to control using microjets. These results are reproduced here to illustrate the principal flow features associated with a supersonic impinging jets and to provide a context for the quantitative BOS results discussed later. These flow visualizations were obtained using a conventional mirror-based, single-pass, white-light shadowgraph method, details of which can be found in [10].

Instantaneous shadowgraph images at TR $= 1.0$ and $h/D = 4$ without and with control are shown in Figs. 3a and 3b, respectively. It may be observed that the impinging jet flowfield without control

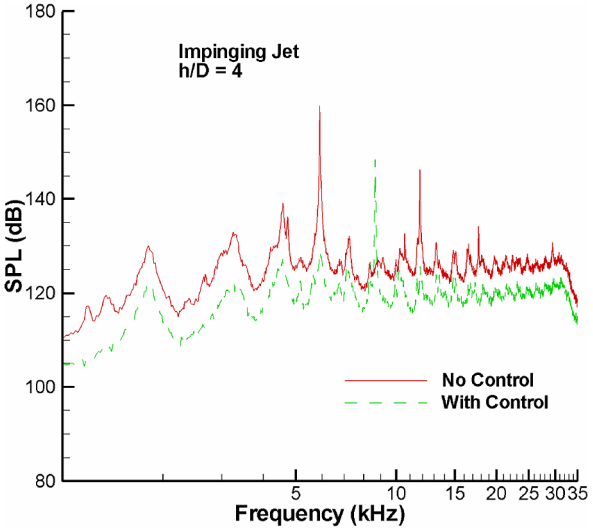

Fig. 4 Impinging jet pressure spectra, $h/D = 4$.

(Fig. 3a) consists of large-scale, azimuthal vortical structures in the jet shear layer along with multiple strong acoustic waves traveling up and down. These impinging and reflecting acoustic waves are the source of high amplitude impingement tones, a characteristic feature of impinging jets. With the activation of microjet based control (Fig. 3b), the flow features are significantly different. First of all, the strength of large-scale azimuthal vortices in the shear layer has been significantly reduced so that they are barely visible in the shadowgraph image. The strong acoustic waves, clearly seen in Fig. 3a, have now been completely eliminated with the activation of control (Fig. 3b). A close and careful examination of the image in Fig. 3b reveals the existence of streamwise streaks in the primary jet, which suggest the presence of streamwise vortices [8]. These qualitative observations are consistent with the quantitative results discussed below.

B. Unsteady Pressure Field

Unsteady pressure measurements were made on the lift plate using a miniature (1/16-in.) Kulite™ pressure transducer (Model No. XCQ-062 and range ±5 psid) located at $2D$ from the nozzle centerline. The transducer signals were conditioned using Stanford™ filters (Model No. SR650) and sampled at 70 kHz. Standard fast Fourier transform (FFT) analysis was used to obtain pressure spectra from these measurements. A total of 100 FFTs of 4096 samples each were averaged to obtain statistically reliable estimate of the narrow-band spectra.

The pressure spectra for impinging jet at a nozzle-to-plate distance $h/D = 4$ with and without control are shown in Fig. 4. The results without control clearly show the presence of multiple, distinct, large amplitude impinging tones and their harmonics. With the activation

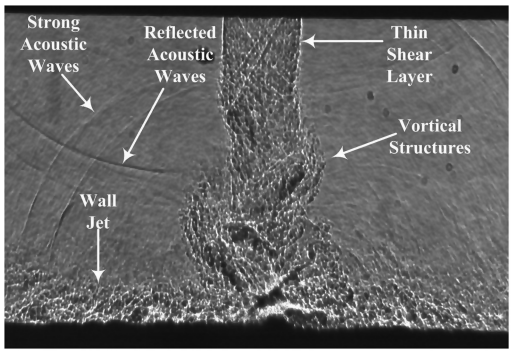

a) No control

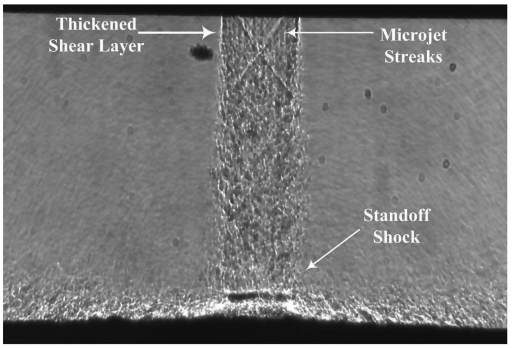

b) With control

Fig. 3 Instantaneous shadowgraph images at TR $= 1.0$, $h/D = 4.0$ (Kumar et al. [10]).

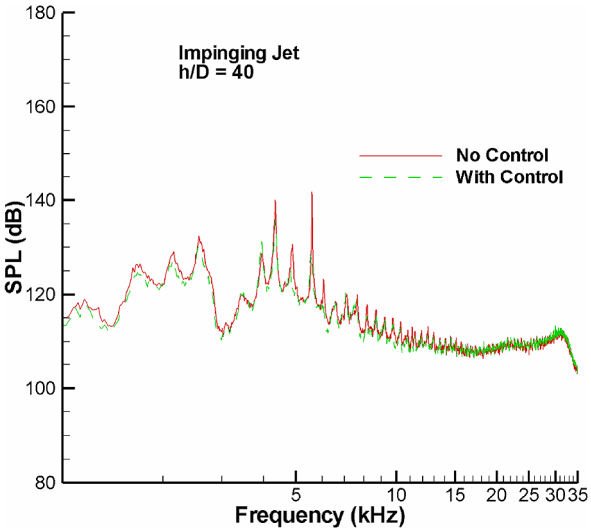

Fig. 5 Free jet pressure spectra, $h/D = 40$.

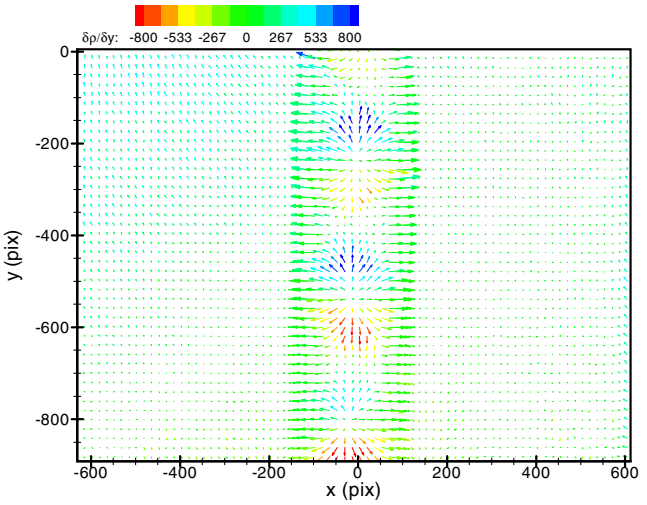

Fig. 7 Average density gradient field obtained by cross-correlation of background dot patterns.

of microjet control, these impinging tones are significantly reduced along with a reduction in broadband levels as well. These results are very similar to those reported in earlier studies [7–10]. The pressure spectra results for the freejet ($h/D = 40$) with and without control are shown in Fig. 5. In contrast to impinging jet, the spectra for freejet is largely broadband in nature with low amplitude tones. This is to be expected as the strong tones present in the case of impinging jets are due to the strong feedback loop resonance [4–10], whereas for free jets the resonance is very weak and the spectra are generally broadband. With the activation of microjet control for free jets, the pressure spectra remains nearly unaltered, except for a small reduction in the tonal amplitude.

C. Results Using BOS

1. Baseline (No Control) Cases

a. Freejet. Figures 6a and 6b show the background images in the absence and presence of flow for the freejet case at NPR = 3.8 (mildly underexpanded). As expected, not much difference can be discerned in the dot patterns.

The gradients of density obtained by cross-correlation of these two images are shown in Fig. 7. The arrows point to the regions of lower density (vectors have been omitted for clarity). The plot shows all the principal features which can be expected in a bidirectional Schlieren with the vectors color coded to the magnitude of the vertical displacement (horizontal knife edge). The plot shows the very mild under expansion due to the imperfect matching of jet exit pressure (NPR = 3.8).

While the case presented here is a freejet ($h/D = 40$), the imaging was carried out over the same streamwise extent, 4D of the jet, for all cases. This gradient field can now be converted to a Poisson type equation, which is solved using established methods to obtain the line-of-sight integrated density field. The filtered back projection tomography (FBPT) technique is then used to extract the density field in the center plane as shown in Fig. 8. As seen here, the normalized density field presented in Fig. 8 clearly captures the regions of high density in the vicinity of the shocks. As expected, Fig. 8 exhibits alternative high and low density regions commensurate with the weakly underexpanded jet. A mild effect of the jet presence is seen on the ambient density field, away from the jet axis.

b. Impinging jet ($h/D = 4$). BOS imaging was carried out for the impinging jet at $h/D = 4$ in a similar manner. Earlier studies [6–9] have shown that at this h/D microjet control was very effective which is why it was chosen as one of the principal test cases.

The density field of the impinging jet was first mapped for the baseline condition, without microjet control. Figure 9 shows the displacement field (also the density gradient field) for this case. The vectors are color coded to the magnitude of the vertical density gradient. The magnitude of the vertical gradient is not calibrated and thus serves only as a qualitative reference to analyze the gradient field. The features corresponding to mild under- expansion are seen again, including the stand-off shock. The features of the wall jet flow on the ground plane are also visualized. The effects of the unsteadiness of the jet impingement are manifested as a blurring of the shear layer near the impingement point. A small outward bulging of the jet about $1D$ downstream ($y = -200$ pix in Fig. 9) of the nozzle is also evident.

The central plane extracted from the normalized density field is presented in Fig. 10. The effect of impingement of the density field is clearly seen, with the stand-off shock appearing as a high density region and a larger impact on the density further from the jet axis compared with the freejet case seen in Fig. 8.

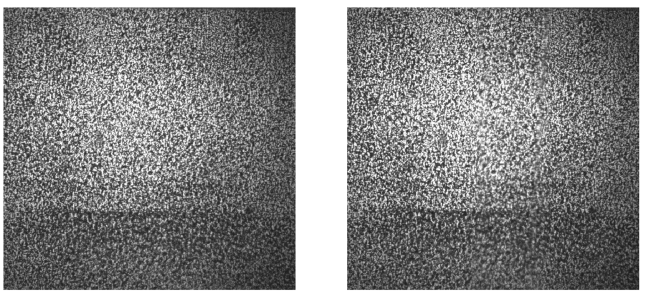

a) No flow **b) With flow**

Fig. 6 Instantaneous background images, $h/D = 40$ (freejet).

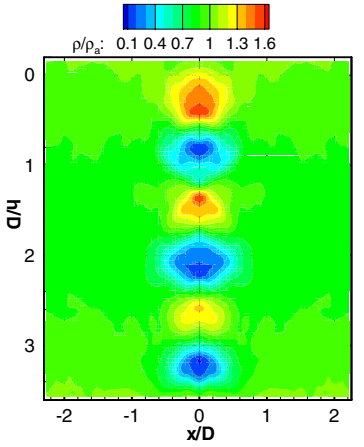

Fig. 8 Normalized density field obtained using BOS in the center plane of for freejet.

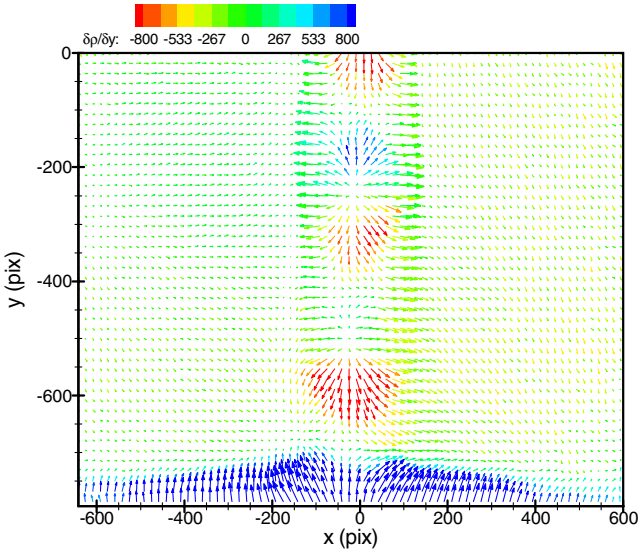

Fig. 9 Average density gradient field for impinging jet, $h/D = 4$.

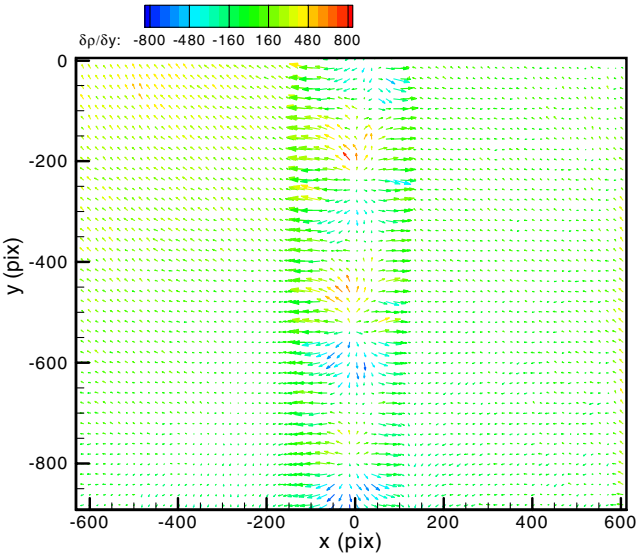

Fig. 11 Average density gradient field for freejet with microjet control.

2. Microjet Control Cases

a. Freejet. The effect of microjet control on the density field can be discerned by examination of Figs. 11 and 12, which present the density gradient field and the center plane of normalized density field, respectively, for the freejet with microjet control. It is immediately obvious that, in addition to a density change near the nozzle exit, the gradient field is significantly different to that shown in Fig. 7. For example, the shock structures are relatively weaker and the jet seems to be steadier with control. This prompts an examination of the normalized density field in the central plane of the jet as shown in Fig. 12. It is seen that here too the density field is significantly different from the density field of the uncontrolled freejet presented earlier in Fig. 8. In particular, at the streamwise station of $h/D = 1.5$, the difference is most evident with the shock cell showing the effect of the microjets at the nozzle exit. This feature is not easily discerned from a conventional Schlieren visualization of this flow, as can be deduced from the density gradient (Schlieren) vector field presented in Fig. 11. This implies that the microjets appreciably change the density field of the freejet. This, when taken in conjunction with the spectra from the unsteady pressure measurements (Fig. 5), which show no significant effect of the microjets on the spectra of the freejet case, raises interesting questions about the nature of this flow. For example, what is the extent of the coupling between the response of the density field and the hydrodynamic and/or near-field acoustic field, where in the former notable changes in the density field were measured with minimal changes in the later. More detailed studies, over a wider parametric range are needed.

b. Impinging jet ($h/D = 4$). The results from the application of BOS for the impinging jet with microjet control are shown in Figs. 13 and 14. The average displacement field, which is also the density gradient field, is presented in Fig. 13. A quick comparison with Fig. 9 shows that the relative magnitudes of the gradients are different and the mild shocks have almost disappeared, despite the data for the microjet control case being from the same experimental run, i.e., the microjets were turned on after imaging the no control case. The absence of the blurred shear layer near the impingement point indicates the much more steady nature of the jet with microjet control, a fact which has been documented in previous investigations of this flow [9,10] using unsteady pressure data. In addition, the bulge in the jet (at $y = -200$ pix) seen in Fig. 9, signifying a very weak underexpansion, has also disappeared with the presence of microjet control.

Figure 14, which plots the density field in the center plane more clearly, depicts some of the significant differences in magnitude from that seen in Fig. 10. The much weakened shock structure is evident as is the greater uniformity of density in the impingement region, which points to a steadier flow. Further, the effect of the impingement on the ambient environment (far away from the jet axis) is less pronounced than it is for the no control case.

Figure 15 shows a comparison of centerline density ($x/D = 0$) for the impinging jet in the absence and presence of control, which have been extracted from the density planes. The plot shows large spatial variations in the time-averaged density for the no control case as is

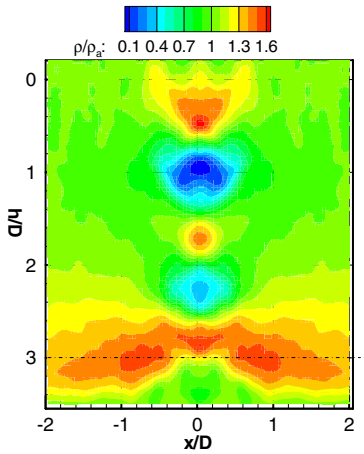

Fig. 10 Center plane of normalized density field for impinging jet obtained using BOS.

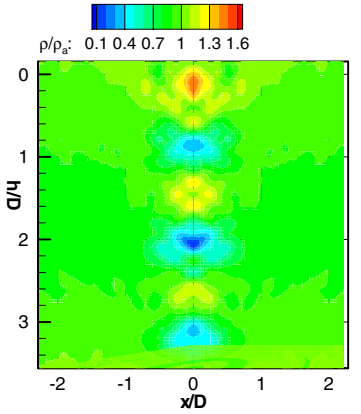

Fig. 12 Center plane of normalized density field for freejet obtained using BOS.

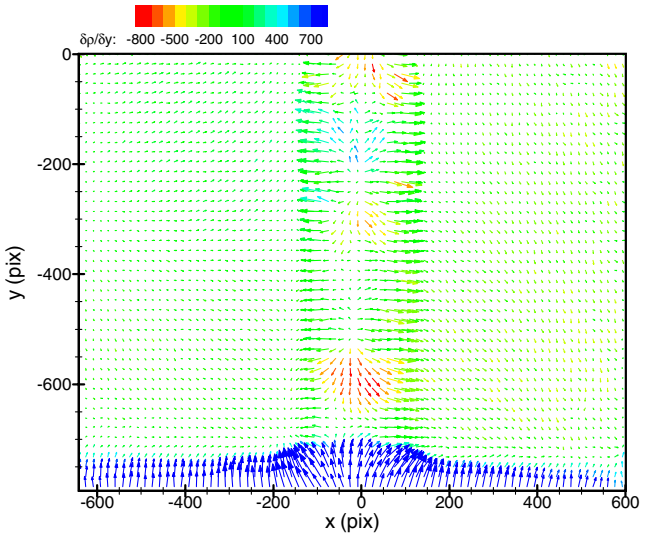

Fig. 13 Average density gradient field for impinging jet with microjet control ($h/D = 4$).

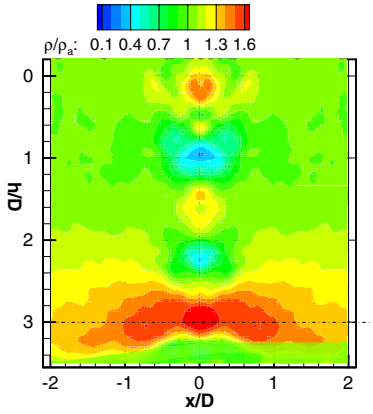

Fig. 14 Center plane of normalized density field for impinging jet with microjet control.

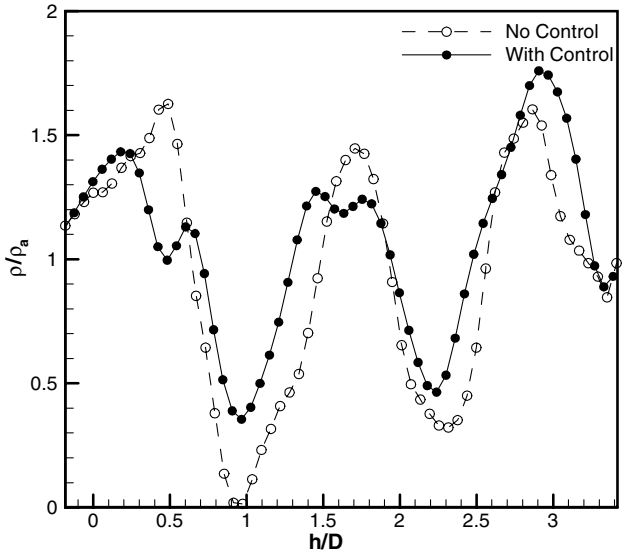

Fig. 15 Effect of microjet control on centerline density variation for impinging jet.

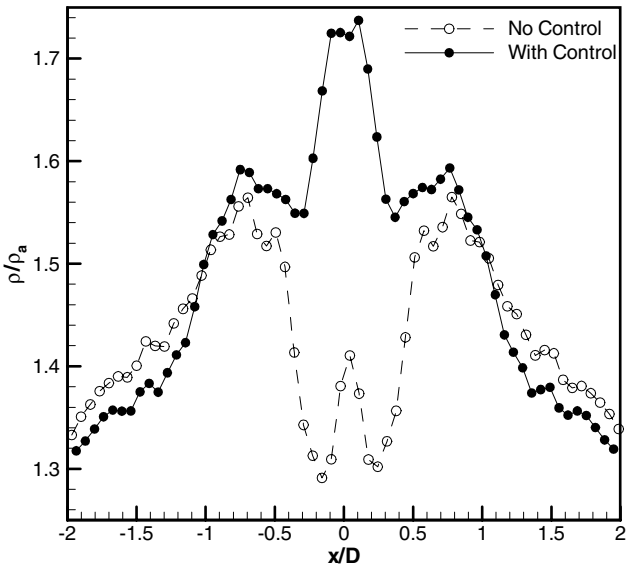

Fig. 16 Effect of microjet control on radial variation of density at $h/D = 3$.

expected for a supersonic impinging jet. When the microjet control is turned on, the amplitude of the variations in density is significantly reduced, signifying a weakening of the shock-cell structure.

As suggested by the density contours in Fig. 14, it is of interest to more closely examine the change in the density field near the impingement region due to the application of control. Figure 16 shows the radial variation of density at a streamwise station of $h/D = 3$ (along dashed lines, Figs. 10 and 14). The figure shows that the radial density distribution has been dramatically altered at this station due to the application of control. The plot indicates a central zone of high density as opposed to the lowered density seen in the no control case, which may be due to the presence of a well defined stand-off shock in case of impinging jet with microjet control. These features were also observed in the shadowgraph images (Fig. 3) and many of the changes in the density field are consistent with our measurements of the velocity field for this flow [9].

IV. Conclusions

This paper describes an initial study where BOS has been applied to the impinging jet flow to document the density field. The aim of the present study is to better understand this flow and its response to control, with the additional density field information that BOS yields. The results show significant changes in the impinging jet density field with the application of control and demonstrate the usefulness of this simple technique in drawing conclusions about the flowfield, in conjunction with other measurements. As observed in prior studies, the effect of the microjets for the impinging case is to lead to a steadier flow, which is captured in the center plane of the normalized density field of the jet plume. In addition, the reduced unsteadiness is also clearly revealed in the density field impingement region at significant distances from the jet axis (along the radial wall jet). This density change in the impinging jet flowfield with control is in accord with the modified unsteady pressure field around the jet and prior velocity field measurements. However, present results for the freejet with control also show measurable changes in the density field, without corresponding changes (of comparable magnitude) in the unsteady pressure field. Detailed studies of the velocity field along with the density field could shed further light on this issue.

Acknowledgment

L. Venkatakrishnan would like to thank the Florida Center for Advanced Aero-Propulsion, for supporting his visit to FSU during the course of this work.

References

[1] Donaldson, C. DuP., and Snedeker, R. S., "A Study of Free Jet Impingement. Part 1. Mean Properties of Free and Impinging Jets," *Journal of Fluid Mechanics*, Vol. 45, 1971, pp. 281–319. doi:10.1017/S0022112071000053

[2] Lamont, P. J., and Hunt, B. L., "The Impingement of Underexpanded Axisymmetric Jets on Perpendicular and Inclined Flat Plates," *Journal of Fluid Mechanics*, Vol. 100, 1980, pp. 471–511. doi:10.1017/S0022112080001255

[3] Ho, C. M., and Nosseir, N. S., "Dynamics of an Impinging Jet. Part 1. The feedback Phenomenon," *Journal of Fluid Mechanics*, Vol. 105, 1981, pp. 119–142. doi:10.1017/S0022112081003133

[4] Alvi, F. S., and Iyer, K. G., "Mean and Unsteady Flowfield Properties of Supersonic Impinging Jets with Lift Plates," AIAA Paper 99-1829, 1999.

[5] Krothapalli, A., Rajkuperan, E., Alvi, F. S., and Lourenco, L., "Flow Field and Noise Characteristics of a Supersonic Impinging Jet," *Journal of Fluid Mechanics*, Vol. 392, 1999, pp. 155–181. doi:10.1017/S0022112099005406

[6] Elavarasan, R., Krothapalli, A., Venkatakrishnan, L., and Lourenco, L., "Suppression of Self-Sustained Oscillations in a Supersonic Impinging Jet," *AIAA Journal*, Vol. 39, No. 12, 2001, pp. 2366–2373. doi:10.2514/2.1243

[7] Alvi, F. S., Shih, C., and Krothapalli, A., "Active Control of the Feedback Loop in High-Speed Jets," AIAA Paper 2001-0373, 2001.

[8] Alvi, F. S., Shih, C., Elavarasan, R., Garg, G., and Krothapalli, A., "Control of Supersonic Impinging Jet Flows Using Supersonic Microjets," *AIAA Journal*, Vol. 41, No. 7, 2003, pp. 1347–1355. doi:10.2514/2.2080

[9] Alvi, F. S., Lou, H., Shih, C., and Kumar, R., "Experimental Study of Physical Mechanisms in the Control of Supersonic Impinging Jets Using Microjets," *Journal of Fluid Mechanics*, Vol. 613, 2008, pp. 55–83. doi:10.1017/S0022112008003091

[10] Kumar, R., Lazic, S., and Alvi, F. S., "Control of High-Temperature Supersonic Impinging Jets Using Microjets," *AIAA Journal*, Vol. 47, No. 12, Dec. 2009, pp. 2800–2811. doi:10.2514/1.39061

[11] Venkatakrishnan, L., and Meier, G. E. A., "Density Measurements Using Background Oriented Schlieren Technique," *Experiments in Fluids*, Vol. 37, No. 2, 2004, pp. 237–247. doi:10.1007/s00348-004-0807-1

[12] Venkatakrishnan, L., "Density Measurements in an Axisymmetric Underexpanded Jet Using Background Oriented Schlieren Technique," *AIAA Journal*, Vol. 43, No. 7, 2005, pp. 1574–1579. doi:10.2514/1.12647

[13] Venkatakrishnan, L., and Suriyanarayanan, P., "Density Field of Supersonic Separated Flow Past an Afterbody Nozzle Using Tomographic Reconstruction of BOS Data," *Experiments in Fluids*, Vol. 47, No. 3, 2009, pp. 463–473. doi:10.1007/s00348-009-0676-8

[14] Meier, G. E. A., "Computerized Background Oriented Schlieren," *Experiments in Fluids*, Vol. 33, 2002, pp. 181–187. doi:10.1017/s00348-002-0450-7

N. Chokani
Associate Editor